






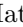
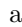



Exploring the accuracy of the equation-of-motion coupled-cluster band gap of solids

Evgeny Moerman ^{1,*} Henrique Miranda ² Alejandro Gallo ³ Andreas Irmler ³ Tobias Schäfer ³
Felix Hummel ³ Manuel Engel ² Georg Kresse ^{2,4} Matthias Scheffler ¹ and Andreas Grüneis ³

¹The NOMAD Laboratory at the FHI of the Max-Planck-Gesellschaft

²VASP Software GmbH, Berggasse 21, A-1090, Vienna, Austria

³Institute for Theoretical Physics, TU Wien, Wiedner Hauptstraße 8–10/136, 1040 Vienna, Austria

⁴University of Vienna, Faculty of Physics, Kolingasse 14, A-1090 Vienna, Austria

(Dated: February 3, 2025)

While the periodic equation-of-motion coupled-cluster (EOM-CC) method promises systematic improvement of electronic band gap calculations in solids, its practical application at the singles and doubles level (EOM-CCSD) is hindered by severe finite-size errors in feasible simulation cells. We present a hybrid approach combining EOM-CCSD with the computationally efficient GW approximation to estimate thermodynamic limit band gaps for several insulators and semiconductors. Our method substantially reduces required cell sizes while maintaining accuracy. Comparisons with experimental gaps and self-consistent GW calculations reveal that deviations in EOM-CCSD predictions correlate with reduced single excitation character of the excited many-electron states. Our work not only provides a computationally tractable approach to EOM-CC calculations in solids but also reveals fundamental insights into the role of single excitations in electronic-structure theory.

Introduction. — The electronic band gap is an important quantity in semiconductor physics and materials science, *i.e.* a fundamental measure of a material’s optical and electronic properties. While density functional theory (DFT) is the state-of-the-art computational method for the electronic structure of materials, its predictive power for band gaps is limited. Local and semi-local exchange-correlation density functional approximations (DFAs) significantly underestimate band gaps [1]. Non-local functionals that include a fraction of exact exchange can improve accuracy but often require the tuning of parameters. The GW approximation [2, 3], particularly in its non-iterative G_0W_0 form, has emerged as the state-of-the-art method for band structure calculations. However, G_0W_0 results are sensitive to the choice of the underlying DFA, known as the starting-point dependence [4, 5].

To obtain accurate electronic band gaps, more advanced methods that systematically incorporate higher orders of electronic correlation effects are needed. Currently, one is left with a choice between three methods. The first one consists in the self-consistent solution of Hedin’s equations (GW) in combination with an additional vertex correction in the screened interaction, that is neglected in G_0W_0 . The resulting method, known as $GW^{\text{TC-TC}}$, has been shown to yield good agreement with experimental band gaps [6]. One must emphasize that in the $GW^{\text{TC-TC}}$ method only the quasi-particle energies are treated self-consistently while for the orbitals the single-particle states of the initial mean-field method (in this work the HSE06 DFA [7]) are not updated. The high accuracy of $GW^{\text{TC-TC}}$ can only be inferred by comparing to experimental gaps properly corrected for zero-point renormalization (ZPR) [8–10]. Quantum Monte

Carlo (QMC) methods offer an alternative avenue to obtain a highly accurate description of electronic correlation. While QMC ground state energies often serve as benchmark results, their application to the electronic band gap of materials has been explored only very recently [11, 12]. Similarly new to the field of materials science, is the equation-of-motion coupled-cluster (EOM-CC) method [13], which has been used to study both neutral [14–16] and charged excitations [17, 18] in solids. In both, the QMC and EOM-CC studies the most challenging obstacle to obtain well converged band gaps was identified to be the finite-size error. This error decays relatively slowly with respect to the employed super cell size or k -point mesh used to sample the Brillouin zone of the primitive unit cell. To better understand the corresponding scaling law, we previously derived the leading order contributions to the finite-size error of the EOM-CC band gap [19]. On top of that, we verified numerically that the finite-size error of both the G_0W_0 and the EOM-CCSD band gap converge with the same rate, which motivates a hybrid approach, in which the convergence behavior can firstly be determined using the substantially cheaper G_0W_0 method and subsequently be employed for the extrapolation of the EOM-CCSD band gap. Here, we apply this new technique to estimate the fundamental EOM-CCSD band gap of a number of insulators and semiconductors.

Method. — To calculate the electronic band gap in the CC theoretical framework, we employ the ionization potential (IP)- and electron affinity (EA)-EOM-CC method. In the case of periodic solids, the IP and EA correspond to the quasi-particle energies of valence and conduction bands, respectively. Here, we provide a succinct summary of the EOM-CC theory. For a detailed account of the electronic structure factor in EOM-CC theory, which is crucial for the derivation of the scaling law of the band gap with respect to system size, see Ref. [19] and references therein.

* moerman@fhi-berlin.mpg.de

The EOM-CC methodology is based on the *similarity-transformed Hamiltonian* $\hat{H} = e^{-\hat{T}} \hat{H} e^{\hat{T}}$, where \hat{T} is the *cluster operator* of ground-state CC theory and \hat{H} is the electronic Hamiltonian. The wave function of the n -th excited state of the charged system $|\Psi_n^{N\mp 1}\rangle$ is obtained by applying an excitation operator $\hat{R}_n^{\text{IP/EA}}$ to $|\Psi_0\rangle$, which is the ground-state wave function of CC theory [13]:

$$|\Psi_n^{N\mp 1}\rangle = \hat{R}_n^{\text{IP/EA}} |\Psi_0\rangle. \quad (1)$$

The \hat{R}_n^{IP} and \hat{R}_n^{EA} operators in the EOM-CC method with single- and double excitations (EOM-CCSD) are $\hat{R}_n^{\text{IP}} = \sum_i r_{i,n} \hat{a}_i + \sum_{ij,a} r_{ij,a}^a \hat{a}_i^\dagger \hat{a}_j$ and $\hat{R}_n^{\text{EA}} = \sum_a r_n^a \hat{a}_a^\dagger + \sum_{iab} r_{i,n}^{ab} \hat{a}_a^\dagger \hat{a}_b^\dagger \hat{a}_i$, respectively. The indices i, j and a, b denote occupied and virtual orbitals. In the case of Bloch orbitals, the orbital index serves as compound index for the k -vector of the primitive unit cell and band number.

IP/EA-EOM-CCSD excitation energies are determined as the eigenvalues of \hat{H} :

$$\hat{H}(\hat{R}_n^{\text{IP/EA}} |\Phi_0\rangle) = E_n^{\text{IP/EA}} (\hat{R}_n^{\text{IP/EA}} |\Phi_0\rangle), \quad (2)$$

whereas $r_{i,n}$, $r_{ij,n}^a$ and r_n^a , $r_{i,n}^{ab}$ represent excited many-electron states. The fundamental electronic band gap is given by the sum between the first IP and EA excitation energies

$$E_{\text{gap}}^{\text{EOM}} = E^{\text{IP}} + E^{\text{EA}}. \quad (3)$$

Note that we have dropped the state index n for brevity. One useful metric to classify EOM-CC excitations is the *single excitation character* defined as

$$n_1^{\text{IP}} = \sum_i r_i^2 \quad n_1^{\text{EA}} = \sum_a (r^a)^2. \quad (4)$$

Especially for low-order truncations of EOM-CC theory, like the EOM-CCSD method, values of $n_1^{\text{IP/EA}}$ close to 1 are associated with an increased accuracy [20].

In this work we employ an efficient extrapolation approach that links the scaling of EOM-CC and G_0W_0 gaps with respect to super cell size. We first perform a series of G_0W_0 band gap calculations sampling the first Brillouin zone employing a k -mesh with a total of N_k points. These G_0W_0 band gaps are fitted to

$$E_{\text{gap},N_k}^{G_0W_0} = E_{\text{gap,TDL}}^{G_0W_0} + AN_k^{-\frac{1}{3}} + BN_k^{-\frac{2}{3}} + CN_k^{-1}. \quad (5)$$

Although the above equation was derived for EOM-CCSD band gaps ($E_{\text{gap}}^{\text{EOM}}$), we find that it works well for G_0W_0 [19]. This can partly be attributed to the fact that the G_0W_0 and EOM-CCSD methods are closely related, which was elucidated in Refs. [21, 22]. We emphasize that there exist well established corrections to the finite-size error in the G_0W_0 band gap, which are referred to as head- and wing-corrections [23]. Here, however, we take advantage of the similar finite-size scaling in G_0W_0 and EOM-CCSD theory by proceeding without these corrections. In the thermodynamic limit (TDL), that is for

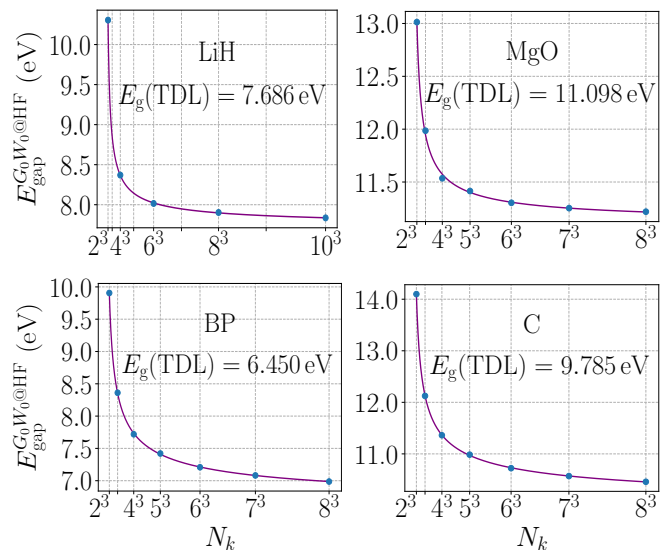


FIG. 1. Scaling of the G_0W_0 @HF band gaps of LiH, MgO, BP and C with respect to the k -mesh using FHI-aims (NAOs). The data points were fitted and extrapolated using the expression $E_{\text{gap},N_k}^{G_0W_0@HF} = E_{\text{gap,TDL}}^{G_0W_0@HF} + AN_k^{-1/3} + BN_k^{-2/3} + CN_k^{-1}$ (see Eq. (5)). $E_g(\text{TDL})$ is a shorthand for $E_{\text{gap,TDL}}^{G_0W_0@HF}$, *i.e.* using a converged k summation.

$N_k \rightarrow \infty$, the G_0W_0 and EOM-CCSD band gaps are strictly linked by [19]

$$E_{\text{gap},N_k}^{\text{EOM}} = a + b \cdot E_{\text{gap},N_k}^{G_0W_0}. \quad (6)$$

The assumption of the present approach is that the above equation already holds approximately for smaller system sizes, which is corroborated by the findings summarized in the next section. Once the system specific fit parameters a and b are obtained using relatively small N_k , one can estimate the EOM-CCSD gap in the TDL by $E_{\text{gap,TDL}}^{\text{EOM}} = a + b \cdot E_{\text{gap,TDL}}^{G_0W_0}$, which follows from the linear scaling relation given above. We note that for G_0W_0 calculations k -summations are performed using k -meshes that correspond to the super cells used for the EOM-CCSD calculations. Furthermore the G_0W_0 calculations in the above procedure employ the same Hartree-Fock (HF) single-particle energies and wave functions (G_0W_0 @HF).

Results. — We now assess the system size convergence of the G_0W_0 band gaps and their extrapolation to the TDL based on Eq. (5). Figure 1 shows that the computed G_0W_0 band gaps are well approximated by Eq. (5) previously derived for IP/EA-EOM-CCSD energies, indicating that both methods yield band gaps that converge to the TDL with the same scaling behaviour. This is supported by Lange and Berkelbach[21], who showed that the G_0W_0 @HF and IP- and EA-EOM-CCSD approximations feature identical low-order ring terms that also play an important role for long-range correlation effects in the ground state [24]. In contrast to the ground-state CC cor-

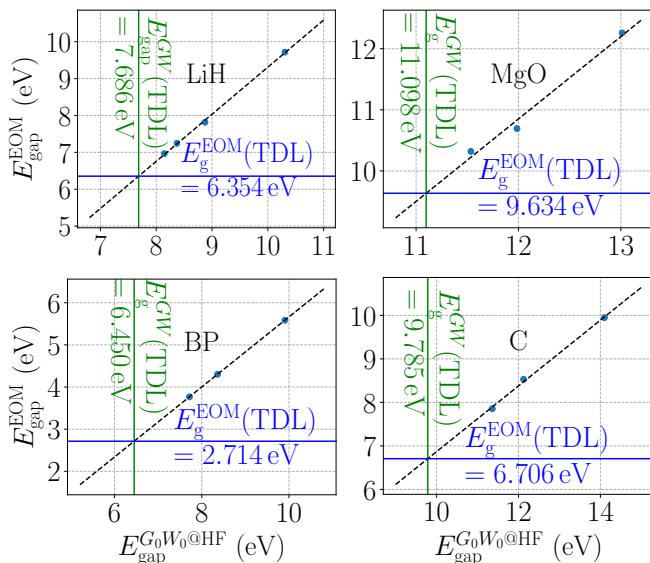


FIG. 2. Correlation of the EOM-CCSD and G_0W_0 @HF band gap convergence of LiH, MgO, BP and C with increasing super cell size (EOM-CCSD) and k -mesh density (G_0W_0 @HF) using FHI-aims. The extrapolated TDL value of the G_0W_0 @HF and of the EOM-CCSD band gap is denoted by $E_{\text{g}}^{G_0W_0}$ (TDL) and $E_{\text{g}}^{\text{EOM}}$ (TDL) and marked by green and blue lines, respectively. The number of k -points increases from $2 \times 2 \times 2$, over $3 \times 3 \times 3$ to $4 \times 4 \times 4$. For LiH results for $5 \times 5 \times 5$ are also shown.

relation energy, which is known to converge to the TDL with a $1/N_k$ rate for insulators [25, 26], our analysis suggests in general a $1/N_k^{1/3}$ leading-order behavior of the band gap in the large N_k limit [19]. Moreover, additional next-to-leading-order contributions need to be included to model the band gap convergence for relatively small k -meshes. The results above have been obtained using FHI-aims (see the SI for computational details).

The next step in the procedure outlined above lies in determining how the scaling behaviour of the G_0W_0 @HF band gap and the EOM-CCSD band gap are correlated with each other. Figure 2 shows the band gaps of the two methods plotted against each other and fitted according to Eq. (6). Indeed, we find that the data points of the four materials consistently lie on a straight line. The validity of the herein established relation between the two methods is most clear in the case of LiH, where a fourth data point ($5 \times 5 \times 5$) is accessible due to the smaller number of electrons per unit cell. For LiH, all four points align on a straight line. This enables a direct estimation of the EOM-CCSD band gap in the TDL given by $E_{\text{gap,TDL}}^{\text{EOM}} = a + b \cdot E_{\text{gap,TDL}}^{G_0W_0}$ and depicted in the plots of Figure 2 at the intersection point between the linear fit and the green vertical line, which shows $E_{\text{gap,TDL}}^{G_0W_0@HF}$ determined previously in Figure 1. Let us emphasize that our approach only depends on the scaling behavior of the G_0W_0 @HF gap, its absolute value is irrelevant. For C, BP and MgO we find that the ex-

TABLE I. Comparison of EOM-CCSD band gaps calculated using different computer codes: NAO-based FHI-aims and PAW-based VASP results obtained from the linear fit against GW gaps as shown in Figure 2 and S2 and corrected for basis set incompleteness (see discussion in Section S3). PySCF results were taken from Reference [18]. $GW^{\text{TC-TC}}$ results and experimental values are shown for reference. The zero-point renormalized value (w/o ZPR) is shown next to the experimentally observed (obs.) one. All values in eV.

Material	EOM-CCSD		$GW^{\text{TC-TC}}$		Exp.
	VASP ^a	FHI-aims ^b	PySCF	VASP	w/o ZPR (obs.)
LiH	6.25	6.32	5.85	5.52	5.43 (4.99 ^g)
C	5.75	6.15	4.88	5.88	5.80 (5.48 ^c)
BP	2.27	2.38	1.65	2.19	2.26 (2.16 ^f)
MgO	9.52	9.19	8.34	8.10	8.36 (7.83 ^j)
Si	1.29		0.93	1.24	1.23 (1.17 ^d)
BN	6.62		6.45	6.58	6.5 (6.1 ^e)
LiF	16.19		15.43	14.73	15.43 (14.2 ^h)
LiCl	9.90		9.43	9.53	9.94 (9.40 ⁱ)

^a Extrapolating from $n \times n \times n$ super cells with $n=2$ and 3
^b Extrapolating from $n \times n \times n$ super cells with $n=2, 3$ and 4
^c [27], ^d [28], ^e [29], ^f [30], ^g [31, 32], ^h [33], ⁱ [34], ^j [35]

trapolated EOM-CCSD band gap value changes at most 0.3 eV if the extrapolation is performed using the $2 \times 2 \times 2$ and $3 \times 3 \times 3$ data points only, omitting the biggest super cell size of $4 \times 4 \times 4$. To confirm the correctness of the IP- and EA-EOM-CCSD implementation in combination with FHI-aims, a small molecular benchmark was conducted and compared to published results (see Table S4 and S5).

We now turn to the discussion comparing EOM-CCSD band gaps obtained with different implementations. Specifically, we have carried out EOM-CCSD calculations employing electronic Hamiltonians computed by FHI-aims and VASP. These are interfaced implementations [36, 37] using super cells, equivalent to corresponding k -meshes of the primitive unit cell. Additionally, we compare our findings against EOM-CCSD results from a previous PySCF study by Vo, Wang and Berkelbach [18]. PySCF calculations used pseudopotentials optimized for Hartree-Fock and Gaussian-type orbitals (GTOs). VASP employs the frozen core approximation with DFT-PBE core states, but including core-valence exact exchange [38]. The present FHI-aims calculations employ the frozen core approximation only on the level of post-HF theories. Therefore core-valence correlation is neglected in all summarized results, whereas the treatment of core-valence exchange exhibits small inconsistencies. In the complete basis set and thermodynamic limit, the band gaps for the same systems should agree to within remaining uncertainties that derive from, *e.g.*, differences in the frozen core approximation. Indeed, we find that VASP and FHI-aims agree well with each other. Table I shows that for LiH and BP our EOM-CCSD band

gaps computed with FHI-aims and VASP yield excellent agreement to within 0.1 eV. Only for MgO and C, VASP and FHI-aims exhibit discrepancies of about 0.3-0.4 eV. This can be partly attributed to the fact that VASP calculations employed $2 \times 2 \times 2$ and $3 \times 3 \times 3$ super cells only due to computational constraints.

Table I reveals that the differences between the FHI-aims and VASP gaps compared to the PySCF results are significant. For LiH, C, MgO and BP the average absolute difference of the EOM-CCSD gaps between VASP/FHI-aims and PySCF is 0.8 eV, whereas VASP and FHI-aims agree to within 0.2 eV on average. What is the reason for these significant discrepancies? Both works have tried to converge the computed band gaps with respect to accessible basis set and system size. For example, Fig. 2 of Ref. [18] depicts TDL extrapolations of EOM-CCSD band gaps for different basis sets. In agreement with our findings, the basis set convergence of EOM-CCSD band gaps is relatively fast, indicating that the most likely source of the discrepancy are finite-size errors. Both TDL extrapolations shown in our Fig. 2 and Fig. 2 from Ref. [18] look reliable at first sight for the system sizes studied ($2 \times 2 \times 2$ to $4 \times 4 \times 4$). However, we stress that the $N_k^{-1/3}$ TDL extrapolations in Ref. [18] assume that the studied systems are already large enough such that the band gap convergence is dominated by the corresponding leading-order finite-size error. Yet, based on numerical findings for low-dimensional systems, we expect that system sizes of about $8 \times 8 \times 8$ would be needed to observe a convergence that follows the pure $N_k^{-1/3}$ behavior [19]. In fact, employing a $N_k^{-1/3}$ TDL extrapolation of the EOM-CCSD gaps for LiH with VASP and FHI-aims would also exhibit a large discrepancy on the scale of more than 1 eV (see SI). We also note that the approach of Ref. [18] yields band gaps that converge from below with increasing k -mesh densities, whereas our band gaps converge from above. The reason for this different behavior in Refs. [17, 18] is that the underlying HF calculations neglect the integrable singularity contribution of the Coulomb potential in the exchange operator, leading to underestimated HF band gaps. We argue that the finite-size errors in the EOM-CCSD band gap of Ref. [18] are still dominated by the underlying HF finite-size errors, which only partly cancel with EOM-CCSD finite-size errors. In contrast, our finite-size errors originate from post-HF EOM-CCSD terms, which decrease the HF band gap for increasing super cell sizes. The treatment of the singularity of the Coulomb potential strongly affects the finite-size convergence behavior of HF [39] and CC [17, 26] theories. To summarise, we conclude that our GW -scaling EOM-CCSD extrapolation technique efficiently compensates finite-size errors and that the obtained band gaps are more precise than those obtained in a previous study by Vo *et al.* [18].

Before discussing the accuracy of EOM-CCSD band gaps, we briefly focus on $GW^{\text{TC-TC}}$ and the experimental band gaps summarized in Table I. $GW^{\text{TC-TC}}$ cal-

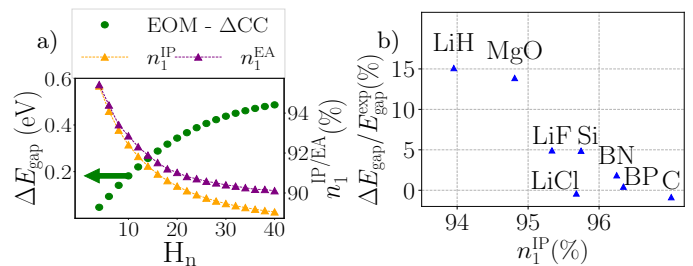


FIG. 3. (a) Single excitation character and gap deviation of EOM-CCSD relative to $\Delta\text{CCSD(T)}$ gap for the molecular hydrogen chain with respect to the chain length. (b) Relation between relative error of EOM-CCSD gap compared to experiment and single excitation character.

culations were performed using the projector augmented wave (PAW) method as implemented in VASP (see the SI for computational details) and are in excellent agreement with ZPR corrected experimental band gaps for all studied systems, confirming Refs. [8, 9]. The employed ZPR correction is explained in Ref. [9] and computational details can be found in the SI. In agreement with recent findings, the ZPR corrections are significant for C and MgO [8]. Here, we show that the ZPR corrections for LiH are also on the scale of about 0.4 eV, substantially larger than previously reported in Ref. [40] and in agreement with experiment [41]. The good agreement between $GW^{\text{TC-TC}}$ and (ZPR corrected) experiment supports our confidence in the correctness of the experimental gaps.

We now turn to the discussion of the accuracy of EOM-CCSD gaps compared to experiment. Note that FHI-aims EOM-CCSD gaps were obtained using larger super cell sizes to verify the reliability of the computationally cheaper VASP EOM-CCSD calculations using smaller super cell sizes. The latter approach could also be applied to a larger number of systems. It is noteworthy that our EOM-CCSD gaps are in excellent agreement with ZPR corrected experimental gaps for C, Si, LiCl, BN and BP. However, the large errors of EOM-CCSD band gaps for LiH, LiF and MgO are unexpected given the accuracy achieved by IP-EOM-CCSD for small molecules compared to experiment, where mean absolute deviations of about 0.15 eV have been observed [20]. Is the EOM-CCSD approximation less accurate for periodic systems than for molecular systems? To address this question, we investigate the single excitation character of the EOM-CCSD states, $n_1^{\text{IP/EA}}$, which has been used in previous studies to explain the performance of a variety of CC methods for molecular IPs [20, 42–44] and neutral double excitations [45]. Before discussing our findings for periodic systems, we demonstrate the significance of $n_1^{\text{IP/EA}}$ using the hypothetical example of dimerized hydrogen chains (H_4 to H_{40}). We compare band gaps calculated via EOM-CCSD against $\Delta\text{CCSD(T)}$ - a refer-

ence method [21, 46] that explicitly computes the ground-state energy of the charged $n + 1$ and $n - 1$ -electron systems thus capturing orbital relaxation effects upon addition/removal of an electron. Using a 20% bond length alternation to ensure insulating behavior, Figure 3a clearly demonstrates that the agreement of EOM-CCSD with $\Delta\text{CCSD(T)}$ deteriorates from 50 meV for H_4 to 0.5 eV for H_{40} . This deviation correlates with a decrease in $n_1^{\text{IP/EA}}$ from 95% to about 90%, highlighting the limitations of EOM-CCSD for extended systems.

Finally, we investigate the relationship between the single excitation character and the deviation of the EOM-CCSD band gap from the experimental value. Figure 3b depicts that we find small relative errors with respect to experiment for n_1^{IP} values above $\approx 95.5\%$, while all materials with a smaller single excitation character (LiH, LiF and MgO) exhibit a sizable disagreement compared to experiment. Figure S7 shows that the single excitation character monotonically decreases with increasing simulation cell size for the IP. The same trend, even though with a smaller magnitude, can be observed for the EA (see Figure S6). In the case of LiH, whose band gap we find to deviate by 0.82 eV from experiment this decrease of n_1^{IP} is the most extreme, dropping by 2%. For MgO, the single excitation character of the IP is also relatively low (94.2%) and comparable to LiH (93.6%). In the case of IP-EOM-CCSD one can clearly see that the magnitude of the single excitation character differ visibly between the materials which are in good agreement with experiment and those which exhibit sizable disagreements in the band gap value. This is strong evidence that the sin-

gle excitation character is a useful quantitative marker to determine whether the EOM-CCSD method yields accurate results for a given system.

Conclusion. — We presented an efficient approach to extrapolate EOM-CCSD band gaps to the TDL using the scaling of G_0W_0 gaps with respect to system size. The precision of this approach was verified through agreement between FHI-aims and VASP calculations, while accuracy was assessed against experimental data and $GW^{\text{TC-TC}}$ results. We found that the EOM-CCSD band gap quality correlates with the single excitation character of the quasi-particle excitation, with accuracy declining significantly for single excitation characters below 95% - a trend confirmed in the alternating hydrogen chain. This paves the way for predictions of band gaps with controllable accuracy. Future work should explore the inclusion higher-order excitation processes in the \hat{T} and \hat{R} operators and the utilization of non-HF-based single particle states to address these limitations.

Acknowledgment. — This project was supported by TEC1p [the European Research Council (ERC) Horizon 2020 research and innovation program, Grant Agreement No.740233] and Grant Agreement No. 101087184. TS acknowledges support from the Austrian Science Fund (FWF) [DOI:10.55776/ESP335]. This work has partly been supported by the European Union Horizon 2020 research and innovation program under the Grant Agreement No 951786 (NOMAD CoE). The computational results presented have partly been achieved using the Vienna Scientific Cluster (VSC) and the Max Plank Computing and Data Facility (MPCDF).

-
- [1] J. P. Perdew, W. Yang, K. Burke, Z. Yang, E. K. Gross, M. Scheffler, G. E. Scuseria, T. M. Henderson, I. Y. Zhang, A. Ruzsinszky, *et al.*, “Understanding band gaps of solids in generalized Kohn–Sham theory,” Proceedings of the national academy of sciences **114**, 2801 (2017).
 - [2] L. Hedin, “New method for calculating the one-particle green’s function with application to the electron-gas problem,” Physical Review **139**, A796 (1965).
 - [3] D. Golze, M. Dvorak, and P. Rinke, “The gw compendium: A practical guide to theoretical photoemission spectroscopy,” Frontiers in chemistry **7**, 377 (2019).
 - [4] P. Rinke, A. Qteish, J. Neugebauer, C. Freysoldt, and M. Scheffler, “Combining GW calculations with exact-exchange density-functional theory: an analysis of valence-band photoemission for compound semiconductors,” New Journal of physics **7**, 126 (2005).
 - [5] F. Fuchs, J. Furthmüller, F. Bechstedt, M. Shishkin, and G. Kresse, “Quasiparticle band structure based on a generalized kohn-sham scheme,” Physical Review B—Condensed Matter and Materials Physics **76**, 115109 (2007).
 - [6] M. Shishkin, M. Marsman, and G. Kresse, “Accurate quasiparticle spectra from self-consistent GW calculations with vertex corrections,” Physical review letters **99**, 246403 (2007).
 - [7] A. V. Krugau, O. A. Vydrov, A. F. Izmaylov, and G. E. Scuseria, “Influence of the exchange screening parameter on the performance of screened hybrid functionals,” The Journal of chemical physics **125** (2006).
 - [8] A. Miglio, V. Brousseau-Couture, E. Godbout, G. Antonius, Y.-H. Chan, S. G. Louie, M. Côté, M. Giantomassi, and X. Gonze, “Predominance of non-adiabatic effects in zero-point renormalization of the electronic band gap,” npj Computational Materials **6**, 167 (2020).
 - [9] M. Engel, H. Miranda, L. Chaput, A. Togo, C. Verdi, M. Marsman, and G. Kresse, “Zero-point renormalization of the band gap of semiconductors and insulators using the projector augmented wave method,” Physical Review B **106**, 094316 (2022).
 - [10] M. Zacharias, M. Scheffler, and C. Carbogno, “Fully anharmonic nonperturbative theory of vibronically renormalized electronic band structures,” Physical Review B **102**, 045126 (2020).
 - [11] R. J. Hunt, M. Szyniszewski, G. I. Prayogo, R. Maezono, and N. D. Drummond, “Quantum monte carlo calculations of energy gaps from first principles,” Physical Review B **98**, 075122 (2018).
 - [12] R. J. Hunt, B. Monserrat, V. Zólyomi, and N. Drummond, “Diffusion quantum monte carlo and GW study of the electronic properties of monolayer and bulk hexag-

- onal boron nitride,” *Physical Review B* **101**, 205115 (2020).
- [13] J. F. Stanton and R. J. Bartlett, “The equation of motion coupled-cluster method. a systematic biorthogonal approach to molecular excitation energies, transition probabilities, and excited state properties,” *The Journal of chemical physics* **98**, 7029 (1993).
- [14] X. Wang and T. C. Berkelbach, “Excitons in solids from periodic equation-of-motion coupled-cluster theory,” *Journal of Chemical Theory and Computation* **16**, 3095 (2020).
- [15] A. M. Lewis and T. C. Berkelbach, “Ab initio linear and pump-probe spectroscopy of excitons in molecular crystals,” *The Journal of Physical Chemistry Letters* **11**, 2241 (2020).
- [16] A. Gallo, F. Hummel, A. Irmeler, and A. Grüneis, “A periodic equation-of-motion coupled-cluster implementation applied to F-centers in alkaline earth oxides,” *J. Chem. Phys.* **154**, 064106 (2021).
- [17] J. McClain, Q. Sun, G. K.-L. Chan, and T. C. Berkelbach, “Gaussian-based coupled-cluster theory for the ground-state and band structure of solids,” *Journal of chemical theory and computation* **13**, 1209 (2017).
- [18] E. A. Vo, X. Wang, and T. C. Berkelbach, “Performance of periodic EOM-CCSD for bandgaps of inorganic semiconductors and insulators,” *The Journal of Chemical Physics* **160** (2024).
- [19] E. Moerman, A. Gallo, A. Irmeler, T. Schäfer, F. Hummel, A. Grüneis, and M. Scheffler, “Finite-size effects in periodic EOM-CCSD for ionization energies and electron affinities: Convergence rate and extrapolation to the thermodynamic limit,” *arXiv preprint arXiv:2409.03721* (2024).
- [20] D. S. Ranasinghe, J. T. Margraf, A. Perera, and R. J. Bartlett, “Vertical valence ionization potential benchmarks from equation-of-motion coupled cluster theory and qtp functionals,” *The Journal of chemical physics* **150** (2019).
- [21] M. F. Lange and T. C. Berkelbach, “On the relation between equation-of-motion coupled-cluster theory and the GW approximation,” *Journal of chemical theory and computation* **14**, 4224 (2018).
- [22] J. Tölle and G. Kin-Lic Chan, “Exact relationships between the GW approximation and equation-of-motion coupled-cluster theories through the quasi-boson formalism,” *The Journal of Chemical Physics* **158** (2023).
- [23] M. S. Hybertsen and S. G. Louie, “Ab initio static dielectric matrices from the density-functional approach. i. formulation and application to semiconductors and insulators,” *Physical Review B* **35**, 5585 (1987).
- [24] R. D. Mattuck, *A guide to Feynman diagrams in the many-body problem*, 2nd ed., Dover books on physics and chemistry (Dover Publications, New York, 1992).
- [25] T. Gruber, K. Liao, T. Tsatsoulis, F. Hummel, and A. Grüneis, “Applying the coupled-cluster ansatz to solids and surfaces in the thermodynamic limit,” *Physical Review X* **8**, 021043 (2018).
- [26] X. Xing and L. Lin, “Inverse volume scaling of finite-size error in periodic coupled cluster theory,” *Physical Review X* **14**, 011059 (2024).
- [27] T. Chiang, *Electronic structure of solids: Photoemission spectra and related data* (Springer, 1989).
- [28] O. Madelung, *Semiconductors: data handbook* (Springer Science & Business Media, 2004).
- [29] M. E. Levinshtein, S. L. Rumyantsev, and M. S. Shur, *Properties of Advanced Semiconductor Materials: GaN, AlN, InN, BN, SiC, SiGe* (John Wiley & Sons, 2001).
- [30] K. Woo, K. Lee, and K. Kovnir, “BP: synthesis and properties of boron phosphide,” *Materials Research Express* **3**, 074003 (2016).
- [31] C. Lushchik, V. Plekhanov, G. Zavt, I. Kuusmann, S. Cholakh, T. Betenekova, P. Liblik, A. O’Connell-Bronin, V. Pustovarov, A. Ratas, *et al.*, “Electronic excitations in LiH and LiD single crystals,” *Eesti NSV Teaduste Akadeemia Füüsika Instituudi uurimused*, 58 (1977).
- [32] S. Baroni, G. P. Parravicini, and G. Pezzica, “Quasiparticle band structure of lithium hydride,” *Physical Review B* **32**, 4077 (1985).
- [33] M. Piacentini, D. W. Lynch, and C. G. Olson, “Thermoreflectance of lif between 12 and 30 ev,” *Phys. Rev. B* **13**, 5530 (1976).
- [34] G. Baldini and B. Bosacchi, “Optical properties of na and li halide crystals at 55 k,” *physica status solidi (b)* **38**, 325 (1970).
- [35] R. Whited, C. J. Flaten, and W. Walker, “Exciton thermoreflectance of MgO and CaO,” *Solid State Communications* **13**, 1903 (1973).
- [36] E. Moerman, F. Hummel, A. Grüneis, A. Irmeler, and M. Scheffler, “Interface to high-performance periodic coupled-cluster theory calculations with atom-centered, localized basis functions,” *The Journal of Open Source Software* **7** (2022).
- [37] F. Hummel, T. Tsatsoulis, and A. Grüneis, “Low rank factorization of the coulomb integrals for periodic coupled cluster theory,” *The Journal of chemical physics* **146** (2017).
- [38] J. Paier, R. Hirschl, M. Marsman, and G. Kresse, “The perdew-burke-ernzerhof exchange-correlation functional applied to the g2-1 test set using a plane-wave basis set,” *The Journal of Chemical Physics* **122**, 234102 (2005).
- [39] R. Sundararaman and T. Arias, “Regularization of the coulomb singularity in exact exchange by Wigner-Seitz truncated interactions: Towards chemical accuracy in nontrivial systems,” *Physical Review B – Condensed Matter and Materials Physics* **87**, 165122 (2013).
- [40] B. Monserrat, N. Drummond, and R. Needs, “Anharmonic vibrational properties in periodic systems: energy, electron-phonon coupling, and stress,” *Physical Review B* **87**, 144302 (2013).
- [41] V. G. Plekhanov, “Isotopic and disorder effects in large exciton spectroscopy,” *Physics-Uspekhi* **40**, 553 (1997).
- [42] A. Shaalan Alag, D. P. Jelenfi, A. Tajti, and P. G. Szalay, “Accurate prediction of vertical ionization potentials and electron affinities from spin-component scaled CC2 and ADC (2) models,” *Journal of Chemical Theory and Computation* **18**, 6794 (2022).
- [43] A. Marie and P.-F. Loos, “Reference energies for valence ionizations and satellite transitions,” *Journal of Chemical Theory and Computation* (2024).
- [44] J. F. Stanton and J. Gauss, “A simple scheme for the direct calculation of ionization potentials with coupled-cluster theory that exploits established excitation energy methods,” *The Journal of chemical physics* **111**, 8785 (1999).
- [45] F. Kossoski, M. Boggio-Pasqua, P.-F. Loos, and D. Jacquemin, “Reference energies for double excitations: Improvement and extension,” *Journal of Chemical The-*

- ory and Computation (2024).
- [46] K. Krause, M. E. Harding, and W. Klopper, “Coupled-cluster reference values for the GW27 and GW100 test sets for the assessment of GW methods,” *Molecular Physics* **113**, 1952 (2015).
- [47] G. Zavit, K. Kalder, I. Kuusman, C. B. Lushchik, and V. Plekhanov, “S. O. cholakh and i? a. e’varestov,” *Sov. Phys. Solid State* **18**, 1588 (1976).
- [48] V.-A. Ha, B. Karasulu, R. Maezono, G. Brunin, J. B. Varley, G.-M. Rignanese, B. Monserrat, and G. Hautier, “Boron phosphide as a p-type transparent conductor: Optical absorption and transport through electron-phonon coupling,” *Physical Review Materials* **4**, 065401 (2020).
- [49] G. Kurbatov, V. Sidorin, K. Sidorin, and A. Sheludchenko, “Diffuse-reflection spectra and electronic structure of BP,” *Fiz. Tekh. Poluprovodn.(Leningrad);(USSR)* **17** (1983).

S1. STRUCTURAL PARAMETERS AND BAND GAP POSITION

TABLE S1: Lattice parameter(s), space group and position of valence band maximum (VBM) and conduction band minimum (CBM) in reciprocal space in relative coordinates for the materials studied in this work.

Material	Lattice parameter (Å)	Space group	\mathbf{k}_{VBM}	\mathbf{k}_{CBM}
LiH	4.084	$Fm\bar{3}m$	(0.0, 0.5, 0.5)	(0.0, 0.5, 0.5)
MgO	4.207	$Fm\bar{3}m$	(0.0, 0.0, 0.0)	(0.0, 0.0, 0.0)
BP	4.538	$F\bar{4}3m$	(0.0, 0.0, 0.0)	(0.0, 0.41 $\bar{6}$, 0.41 $\bar{6}$)
C	3.567	$Fd\bar{3}m$	(0.0, 0.0, 0.0)	(0.0, 0. $\bar{3}$, 0. $\bar{3}$)
BN	3.607	$F\bar{4}3m$	(0.0, 0.0, 0.0)	(0.5, 0.0, 0.5)
Si	5.430	$Fd\bar{3}m$	(0.0, 0.0, 0.0)	(0.41, 0.0, 0.41)
LiCl	5.106	$Fm\bar{3}m$	(0.0, 0.0, 0.0)	(0.0, 0.0, 0.0)
LiF	4.010	$Fm\bar{3}m$	(0.0, 0.0, 0.0)	(0.0, 0.0, 0.0)

The lattice parameters were taken from Table 2 in Reference [1]. The k -shifts for the positions of the conduction band minimum (CBM) and the valence band maximum (VBM) were determined using the PBE-DFA. In the case of diamond (C), the conduction band minimum determined via PBE was found to be at $\approx (0.0, 0.3621, 0.3621)$. Due to limitations of the Hartree-Fock (HF) method in FHI-aims on performing calculations with a shifted k -mesh, k -shifts in FHI-aims had to be performed via down-sampling from a finer mesh. Since the required k -mesh, which would be necessary to down-sample to that k -point would be impractically large, the conduction band minimum of C was evaluated at $\mathbf{k}_{\text{CBM}} = (0.0, 0.\bar{3}, 0.\bar{3})$ as specified in Table S1. The resulting deviation of the band gap was quantified using the PBE-DFA and HF theory and corresponds to 20 meV and 52 meV, respectively. For LiCl and LiF, the valence band maxima predicted by PBE are slightly shifted away from the Γ -point, $\mathbf{k}_{\text{VBM}} = (0.07, 0.07, 0.14)$ for LiCl and $\mathbf{k}_{\text{VBM}} = (0.06, 0.06, 0.11)$ for LiF. Due to the small magnitude of that shift and the very flat dispersion of the valence band around the Γ -point, the EOM-CCSD calculations were performed using the Γ -point as the valence band maximum. On the PBE level of theory this approximation yields a deviation of less than 10 meV. All EOM-CCSD calculations were performed using super cells, for which the k -shifts in Table S1 were scaled appropriately.

S2. COMPUTATIONAL DETAILS

A. FHI-aims

All G_0W_0 @HF and EOM-CCSD calculations to determine the bulk-limit of the EOM-CCSD band gaps were performed using the loc-NAO-VCC-2Z [2] basis set to which a f -, g - and h -type auxiliary basis function of effective charge 1.0 was added manually to ensure sufficient completeness of the auxiliary basis. To perform the CC calculations, the converged HF quantities from FHI-aims were subsequently post-processed by the CC-aims interface [3], which generated the necessary input for the Cc4s software package [4].

To compute the EOM-CCSD band gaps the HF single-particle wave functions were obtained by down-sampling from a k -mesh of size $10 \times 10 \times 10$ or more. This was done because the current implementation of FHI-aims does not allow to perform shifts of the k -mesh in combination with the HF method, which, however, is necessary to sample the conduction band minimum of two of the investigated systems (diamond and boron phosphide). By performing the HF calculation on a denser k -grid and subsequently downsampling the CC calculation to a coarser (and in these cases shifted) grid, this limitation can be circumvented.

The EOM-CCSD finite-size convergence study for LiH involved isotropic supercells of size $2 \times 2 \times 2 - 5 \times 5 \times 5$, while for the other materials $2 \times 2 \times 2 - 4 \times 4 \times 4$ supercells were employed. While the EOM-CCSD band gap was computed at \mathbf{k}_{VBM} and \mathbf{k}_{CBM} from Table S1, due to limitations of the G_0W_0 @HF implementation of FHI-aims, all G_0W_0 calculations related to the study of the band gap finite-size convergence were performed for the direct $\Gamma \rightarrow \Gamma$ band gap.

The BSIE was estimated by performing $2 \times 2 \times 2$ EOM-CCSD super cell calculations at the (appropriately scaled) \mathbf{k}_{VBM} and \mathbf{k}_{CBM} from Table S1 using the loc-NAO-VCC-3Z and -4Z basis sets. For all studied materials, the change of the EOM-CCSD band gap between the 3Z and 4Z was found to be less than 130 meV (see Table S3). Similarly to the BSIE correction performed in the EOM-CCSD study by Vo *et al.* [5], the BSIE in this work was estimated as

the difference between the 2Z basis result used in the study of the finite-size convergence and the 4Z result for the $2 \times 2 \times 2$ super cell and was added to the 2Z-based bulk-limit result of the EOM-CCSD band gap.

To remain consistent with the treatment of the long-range contribution of Coulomb potential in the underlying HF calculations all G_0W_0 and EOM-CCSD calculations were performed using the cut-Coulomb potential [6].

B. VASP

The PAW-based EOM-CCSD calculations involved in the study of the finite-size convergence of the band gap were performed with a basis set of 6 virtual orbitals per occupied orbital ($N_v/N_o = 6$) using super cells of size $2 \times 2 \times 2 - 5 \times 5 \times 5$ for LiH and with $N_v/N_o = 3$ for the $2 \times 2 \times 2$ and $3 \times 3 \times 3$ super cells for MgO, BP and C. In contrast to FHI-aims, VASP does not have a restriction on performing HF calculations for shifted k -meshes, so that no down-sampling was employed. Similar to FHI-aims, the G_0W_0 implementation in VASP is not compatible with shifted k -meshes, so that all GW calculations were performed for the $\Gamma \rightarrow \Gamma$ band gap. The long-range contributions to the Coulomb potential for both EOM-CCSD and the GW calculations were approximated using the probe-charge Ewald method [7].

In analogy to the approach pursued for FHI-aims, the BSIE of the PAW-based calculations was quantified by computing the EOM-CCSD band gap of the $2 \times 2 \times 2$ super cell using the aforementioned basis set of size $N_v/N_o = 6$ (LiH) or $N_v/N_o = 3$ (MgO, BP, C) and a much bigger basis set of $N_v/N_o = 19$, serving as an estimate to the complete basis limit. The BSIE estimate was taken as the difference between the band gap values of these two basis set sizes and is tabulated in Table S3. That difference was added to the finite-size extrapolated EOM-CCSD band gap to obtain the final gap value.

The G_0W_0 @HF calculations were performed employing the single step GW procedure in VASP (available in versions > 6.3), which automatically determines all necessary computational parameters.

Both the G_0W_0 and EOM-CCSD calculations were performed using the `Li_GW`, `H_GW`, `Mg_GW`, `O_GW_new`, `P_GW`, `B_GW` and `C_GW` POTCARs and the maximal recommended kinetic energy cut-off (`ENMAX`) therein.

The self-consistent vertex-corrected GW calculations were performed using the $GW^{\text{TC-TC}}$ implementation in VASP [8]. In contrast to the previously discussed G_0W_0 @HF calculations, the finite-size convergence of the $GW^{\text{TC-TC}}$ calculations was accelerated using head- and wing-corrections. $GW^{\text{TC-TC}}$ for up to $6 \times 6 \times 6$ k -points were performed and extrapolated to the complete basis set limit. The final band gap values are estimated to have a remaining uncertainty of 50 meV.

The zero-point renormalizations (ZPR) were taken directly from Reference [9] while the values for LiH, LiCl and BP were computed following the same perturbative approach. It should be pointed out that in Ref. [9] a lattice parameter of 4.211 Å was used for MgO, 3.536 Å for C and 4.055 Å for LiF. Also, the LDA exchange correlation functional was used for the C calculation and PBE for MgO.

For the LiH, LiCl and BP calculations we used a PBE exchange correlation functional, cutoff energy of 520 eV and supercells made of 3x3x3 copies of the conventional cell and 2x2x2 k -point sampling for BP and LiCl and 3x3x3 k -point sampling for LiH to compute the electron-phonon potential. We included 474 bands for LiH, 934 bands for LiCl and 640 bands for BP in the sum-over-states for the ZPR calculation and a small imaginary complex shift of 0.01 eV. A summary of the parameters and results of the ZPR calculations is shown in Table S2.

TABLE S2: Parameters for the ZPR calculation of BP, LiH and LiCl.

Material	Lattice parameter (Å)	\mathbf{k}_{VBM}	\mathbf{k}_{CBM}	ϵ_{xx}^∞	Z_{xx}^*	ZPR (meV)	POTCAR
BP	4.538	(0.0, 0.0, 0.0)	(0.0, 0.4149, 0.4149)	9.150	0.508	106	<code>B_GW_new</code> <code>P_GW</code>
BP	4.538	(0.0, 0.0, 0.0)	(0.0, 0.4149, 0.4149)	9.158	0.514	105	<code>B_GW</code> <code>P_GW</code>
LiH	4.084	(0.0, 0.5, 0.5)	(0.0, 0.5, 0.5)	4.294	1.027	444	<code>Li_sv_GW</code> <code>H_GW</code>
LiH	4.084	(0.0, 0.5, 0.5)	(0.0, 0.5, 0.5)	4.249	1.027	450	<code>Li_GW</code> <code>H_GW</code>
LiCl	5.106	(0.0, 0.0, 0.0)	(0.0, 0.0, 0.0)	2.979	1.184	543	<code>Li_sv_GW</code> <code>Cl_GW</code>

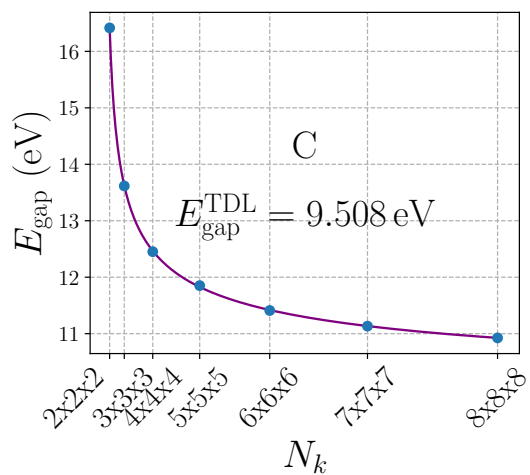
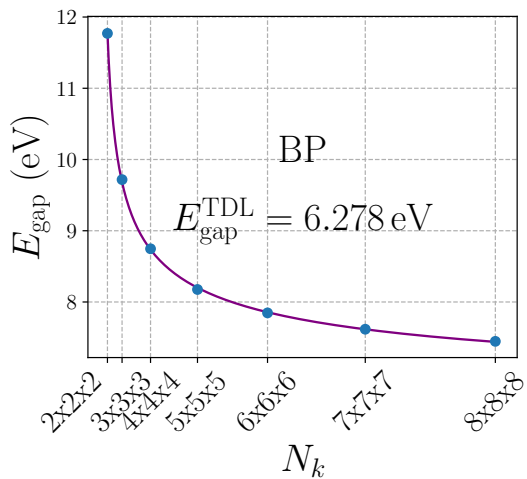
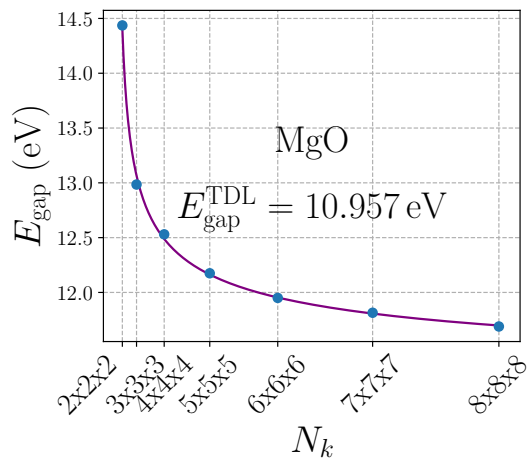
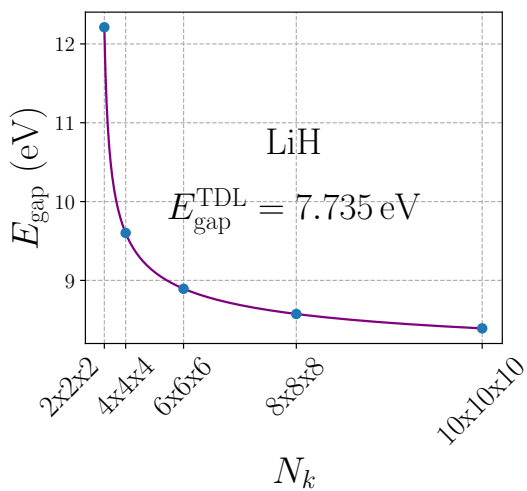
C. NWChem

The calculations of the finite hydrogen chain were performed with a def2-SVP basis set using the NWChem code. Both the IP/EA-EOM-CCSD and the $\Delta\text{CCSD(T)}$ calculations used a spin-restricted HF starting-point, which in the case of the charged $N - 1$ and $N + 1$ systems was given by the spin-restricted open-shell HF (ROHF) wave function and eigenvalues.

S3. ESTIMATION OF THE BASIS SET INCOMPLETENESS ERROR

TABLE S3: Change of $2 \times 2 \times 2$ EOM-CCSD band gap with increasing basis set for FHI-aims and VASP. For FHI-aims, the change of the loc-NAO-VCC-2Z and -3Z based band gap relative to the loc-NAO-VCC-4Z basis set is shown. For VASP the relative change of the EOM-CCSD band gap obtained with $N_v/N_o = 6$ (LiH) or $N_v/N_o = 3$ (MgO, BP, C) compared to a basis set of size $N_v/N_o = 19$ is shown. All entries are in eV.

Material	BSIE wrt. 4Z (FHI-aims)		BSIE wrt. $N_v/N_o = 19$ (VASP)
	2Z	3Z	$N_v/N_o = 3$
LiH	-0.029	0.005	0.089
MgO	-0.446	0.018	0.139
BP	-0.331	-0.057	0.125
C	-0.556	-0.124	0.102
BN	—	—	0.195
Si	—	—	0.170
LiCl	—	—	0.052
LiF	—	—	-0.003

S4. $G_0W_0@HF$ AND EOM-CCSD CONVERGENCE USING THE PAW METHOD

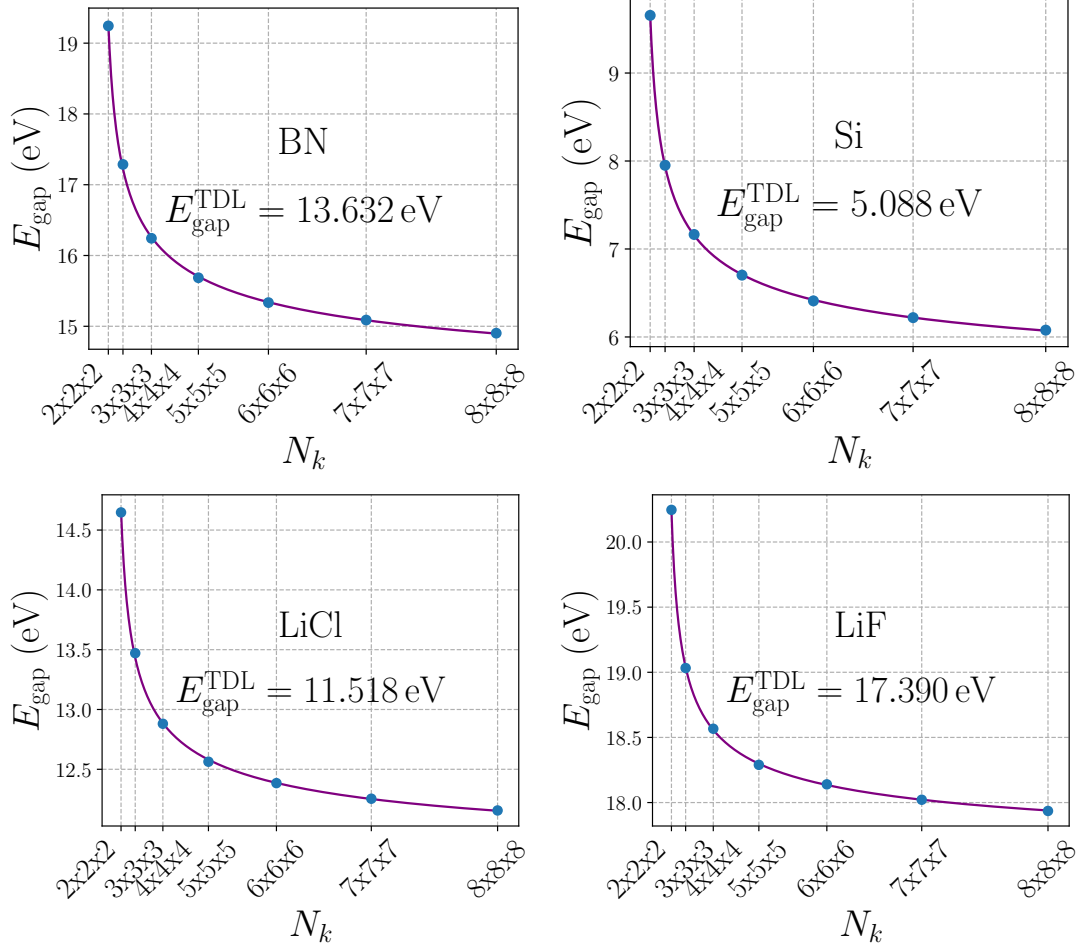
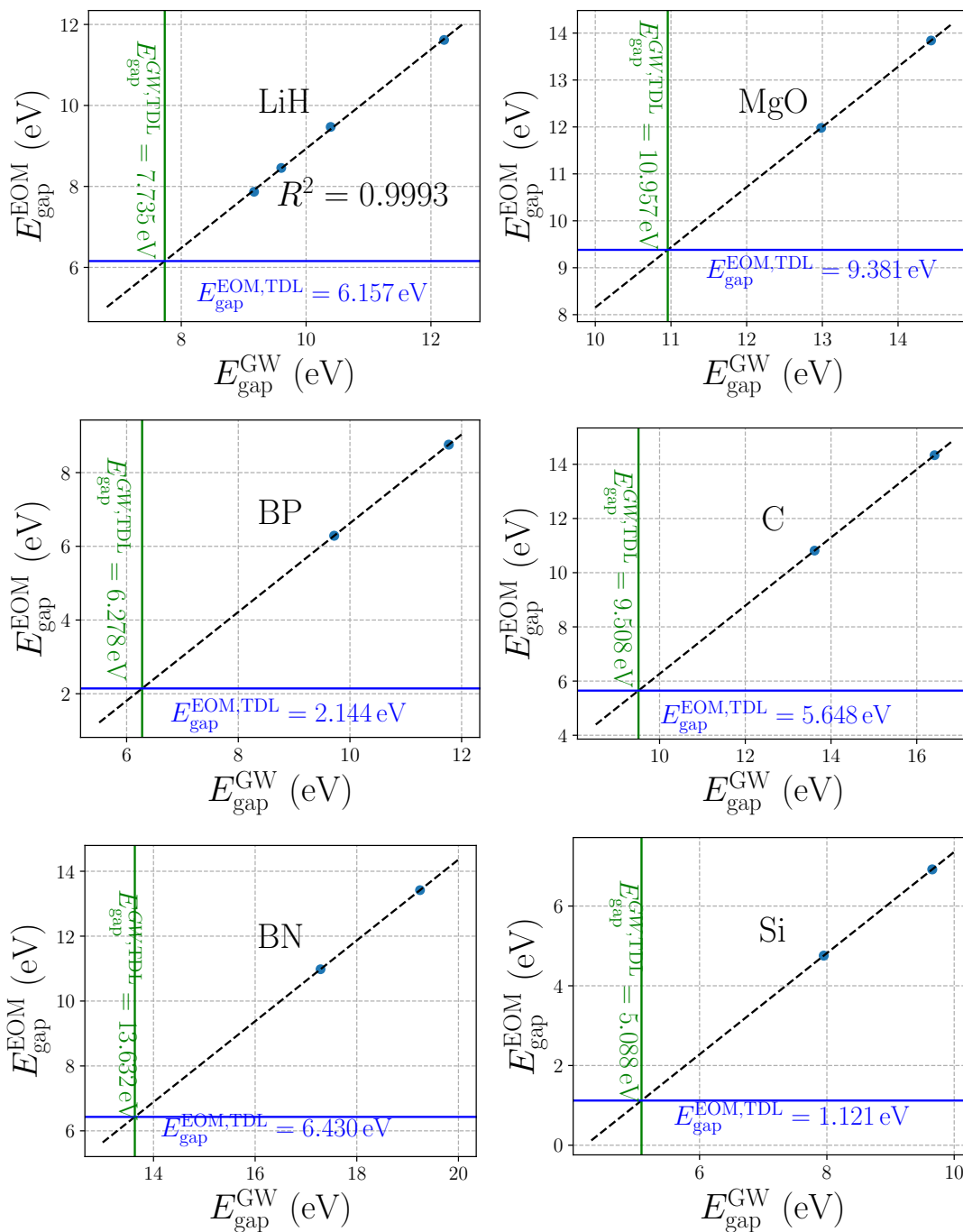


FIG. S1: Convergence of the VASP $G_0W_0@HF$ band gaps with respect to the \mathbf{k} -mesh. The data points were fitted and extrapolated using the expression $E_{\text{gap}}(N_k) = E_{\text{gap}}^{\text{TDL}} + AN_k^{-1/3} + BN_k^{-2/3} + CN_k^{-1}$.



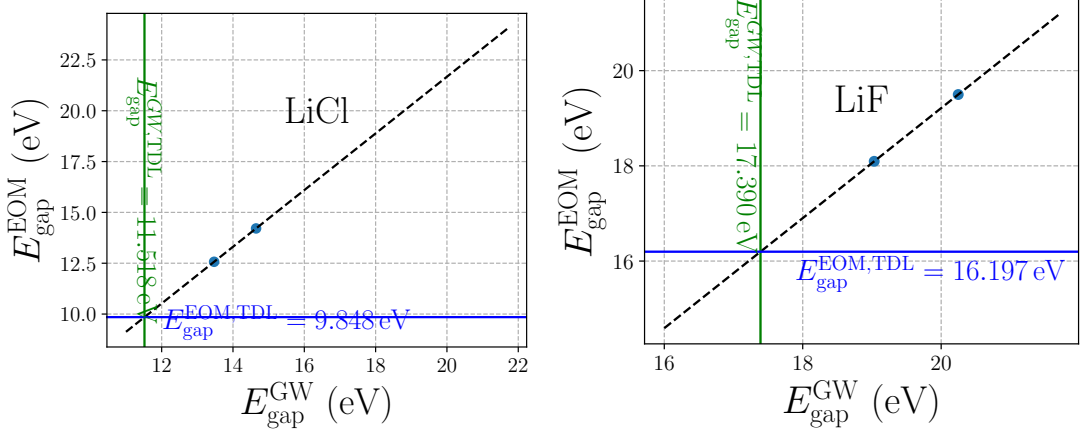


FIG. S2: Correlation of the EOM-CCSD and $G_0W_0@HF$ band gaps convergence using VASP with increasing supercell size (EOM-CCSD) and \mathbf{k} -mesh density ($G_0W_0@HF$). For LiH isotropic supercells of size $2 \times 2 \times 2 - 5 \times 5 \times 5$ were used, while for the other materials $2 \times 2 \times 2$ and $3 \times 3 \times 3$ supercells were employed. For all four systems the band gap converges from above, so that system size increases from right to left. At the TDL value of the GW band gap, obtained in the previous section via extrapolation, a vertical line was drawn. The resulting TDL estimate of the EOM-CCSD band gap is marked by a horizontal line.

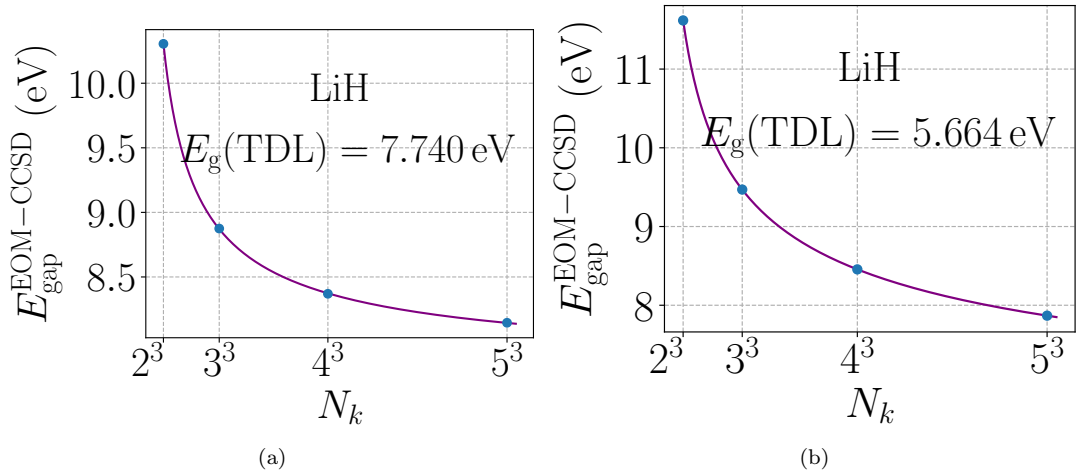


FIG. S3: Convergence of the EOM-CCSD band gap of LiH and extrapolation via $AN_k^{-1/3} + BN_k^{-2/3} + CN_k^{-1}$ based on results from a) FHI-aims and b) VASP

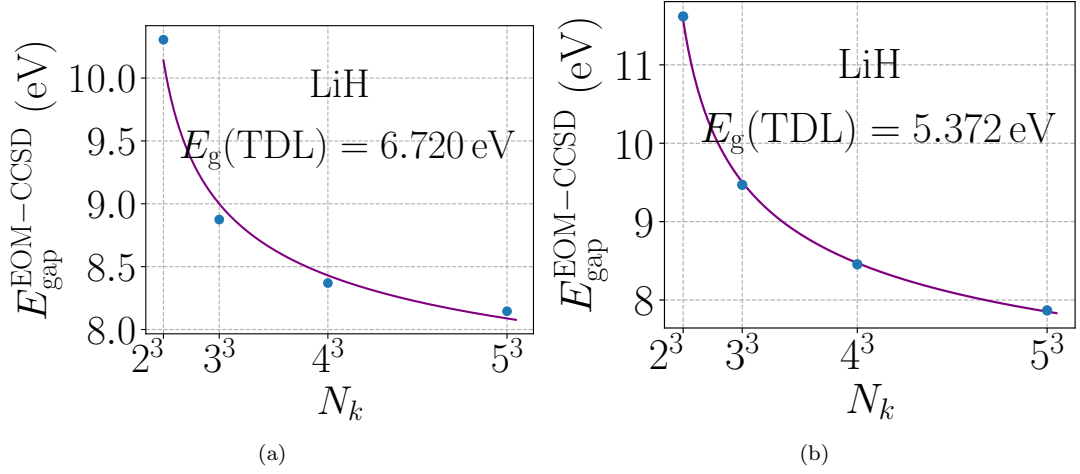


FIG. S4: Convergence of the EOM-CCSD band gap of LiH and extrapolation only via the leading order term $AN_k^{-1/3}$ based on results from a) FHI-aims and b) VASP

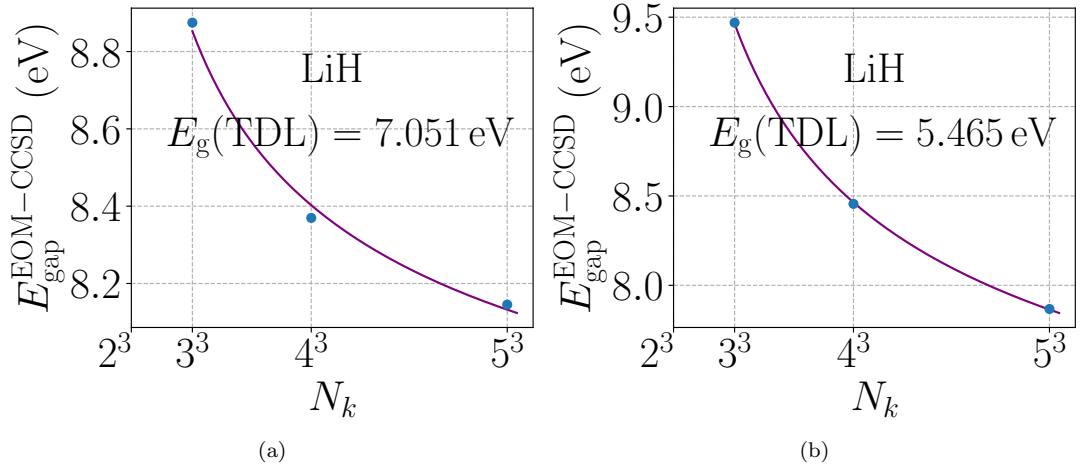


FIG. S5: Convergence of the EOM-CCSD band gap of LiH and extrapolation only via the leading order term $AN_k^{-1/3}$ based on $3 \times 3 \times 3 - 5 \times 5 \times 5$ results from a) FHI-aims and b) VASP

S5. SINGLE EXCITATION CHARACTER OF EA-EOM-CCSD

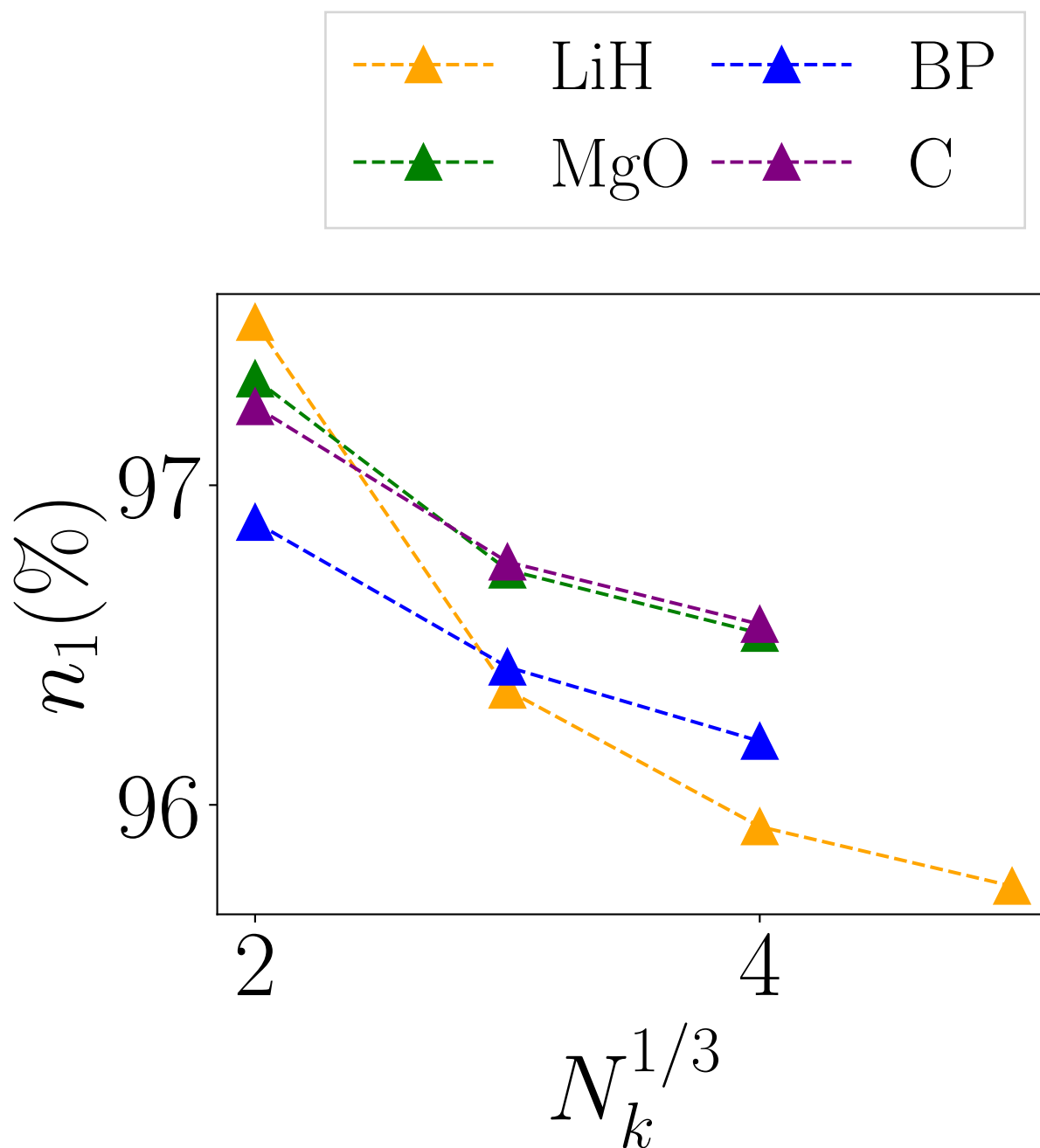


FIG. S6: Change of single excitation character of the EA quasi-particle for the 3D bulk materials with respect to the super cell size.

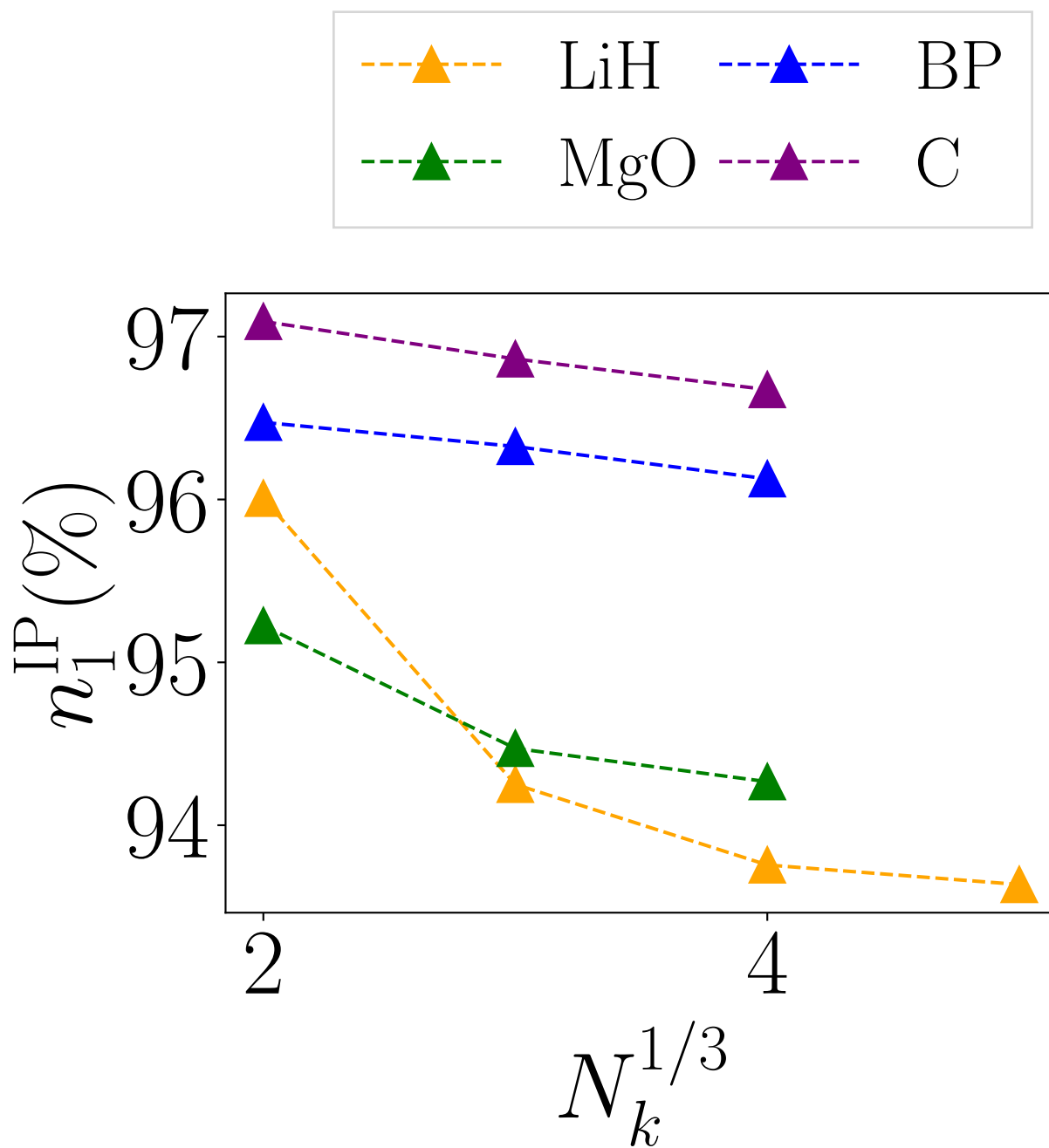


FIG. S7: Change of single excitation character of the IP quasi-particle for the 3D bulk materials with respect to the super cell size.

S6. IP- AND EA-EOM-CCSD BENCHMARK FOR SMALL MOLECULES

system	n	loc-NAO-VCC- n Z	NAO-VCC- n Z	cc-pV n Z [10]	aug-cc-pV n Z [10]
N ₂	2	15.49	15.52	15.18	15.43
	3	15.73	15.64	15.56	15.65
	4	15.69	15.70	15.68	15.71
	CBS		15.75	15.78	15.80
F ₂	2	16.10	15.58	15.10	15.40
	3	15.86	15.66	15.49	15.61
	4	15.81	15.72	15.66	15.72
	CBS		15.76	15.80	15.82
CO	2	14.23	14.09	13.81	13.99
	3	14.29	14.16	14.13	14.18
	4	14.24	14.22	14.22	14.23
	CBS		14.27	14.30	14.30

TABLE S4: Ionization potentials for N₂, F₂ and CO using NAOs and GTOs. The molecular geometries and the the GTO-based values of the ionization potentials were taken from Reference [10]. The CBS extrapolation of the NAO-based results was performed employing a cubic two-point extrapolation expression using the NAO-VCC-3Z and NAO-VCC-4Z result. The results are given in eV.

system	n	loc-NAO-VCC- n Z	NAO-VCC- n Z	cc-pV n Z [11]	aug-cc-pV n Z [11]
C ₂	2	3.10	3.08	2.53	3.13
	3	3.19	3.19	3.07	3.30
	4	3.29	3.26	3.24	3.35
	CBS		3.32	3.34	3.38
O ₃	2	1.63	1.43	0.61	1.57
	3	1.48	1.68	1.31	1.77
	4	1.73	1.76	1.63	1.85
	CBS		1.82	1.82	1.95

TABLE S5: Electron affinities for C₂ and O₃ using NAOs and GTOs. The molecular geometries and the the GTO-based values of the electron affinities were taken from Reference [11]. The CBS extrapolation of the NAO-based results was performed employing a cubic two-point extrapolation expression using the NAO-VCC-3Z and NAO-VCC-4Z result. The results are given in eV.

-
- [1] A. Grüneis, M. Marsman, and G. Kresse, “Second-order möller–plesset perturbation theory applied to extended systems. ii. structural and energetic properties,” *The Journal of Chemical Physics* **133** (2010).
 - [2] I. Y. Zhang, A. J. Logsdail, X. Ren, S. V. Levchenko, L. Ghiringhelli, and M. Scheffler, “Main-group test set for materials science and engineering with user-friendly graphical tools for error analysis: systematic benchmark of the numerical and intrinsic errors in state-of-the-art electronic-structure approximations,” *New Journal of Physics* **21**, 013025 (2019).
 - [3] E. Moerman, F. Hummel, A. Grüneis, A. Irmeler, and M. Scheffler, “Interface to high-performance periodic coupled-cluster theory calculations with atom-centered, localized basis functions,” *The Journal of Open Source Software* **7** (2022).
 - [4] “cc4s; available from <https://manuals.cc4s.org>.” Accessed on 01.05.2025.
 - [5] E. A. Vo, X. Wang, and T. C. Berkelbach, “Performance of periodic eom-ccsd for bandgaps of inorganic semiconductors and insulators,” *The Journal of Chemical Physics* **160** (2024).
 - [6] S. V. Levchenko, X. Ren, J. Wieferink, R. Johanni, P. Rinke, V. Blum, and M. Scheffler, “Hybrid functionals for large periodic systems in an all-electron, numeric atom-centered basis framework,” *Computer Physics Communications* **192**, 60 (2015).
 - [7] S. Massidda, M. Posternak, and A. Baldereschi, “Hartree-fock lapw approach to the electronic properties of periodic systems,” *Physical Review B* **48**, 5058 (1993).
 - [8] M. Shishkin, M. Marsman, and G. Kresse, “Accurate quasiparticle spectra from self-consistent gw calculations with vertex corrections,” *Physical review letters* **99**, 246403 (2007).
 - [9] M. Engel, H. Miranda, L. Chaput, A. Togo, C. Verdi, M. Marsman, and G. Kresse, “Zero-point renormalization of the band gap of semiconductors and insulators using the projector augmented wave method,” *Physical Review B* **106**, 094316 (2022).
 - [10] M. Musiał, S. A. Kucharski, and R. J. Bartlett, “Equation-of-motion coupled cluster method with full inclusion of the connected triple excitations for ionized states: Ip-eom-ccsdt,” *The Journal of chemical physics* **118**, 1128 (2003).
 - [11] M. Musiał and R. J. Bartlett, “Equation-of-motion coupled cluster method with full inclusion of connected triple excitations for electron-attached states: Ea-eom-ccsdt,” *The Journal of chemical physics* **119**, 1901 (2003).